INTERNATIONAL JOURNAL OF CLIMATOLOGY
Int. J. Climatol. (2014)
Published online in Wiley Online Library
(wileyonlinelibrary.com) DOI: 10.1002/joc.3930

RMetS
Royal Meteorological Society

Hydrological links in Southeastern South America: soil moisture memory and coupling within a hot spot

R. C. Ruscica,[a]* A. A. Sörensson[a] and C. G. Menéndez[a,b]
[a] *Centro de Investigaciones del Mar y la Atmósfera (CIMA), CONICET/UBA, Buenos Aires, Argentina*
[b] *Departamento de Ciencias de la Atmósfera y los Océanos, FCEN, UBA, Buenos Aires, Argentina*

ABSTRACT: Southeastern South America has been identified as a hot spot of soil moisture and evapotranspiration coupling efficiency during austral summer in a previous study. Here, hydrological processes such as coupling and memory of soil moisture, evapotranspiration and precipitation and the links between these variables are discussed on the daily time scale over this region. The correlations between surface variables, rainfall persistence and soil moisture memory are discussed over three subregions selected on basis of their coupling efficiency and mean daily intensity of precipitation. The relationship between surface climate and land cover is qualitatively assessed. The memory, or statistical persistence, is longer and has a more robust spatial pattern for the root zone than for the top soil moisture. Where the coupling efficiency between soil moisture and evapotranspiration is high, the evapotranspiration is regulated by soil moisture conditions independently on the intensity of precipitation, whereas in a region with low coupling efficiency and high intensity, the evapotranspiration is regulated by the atmosphere. The coupling efficiency is in general related to the memory of the root-zone layer, since the soil state is modified when the soil moisture and the atmosphere interact, resulting in an anticorrelation between these metrics. The persistence of rainfall is another factor that modulates the memory. Nevertheless, there are some areas around the La Plata River where both the coupling efficiency and the memory are relatively high, such as Uruguay and the northeast of Argentina, where an improvement of soil moisture initial conditions could improve predictability of surface variables on a monthly timescale.

KEY WORDS soil moisture memory; evapotranspiration; precipitation; Southeastern South America; La Plata Basin; regional climate modelling

Received 30 March 2013; Revised 26 November 2013; Accepted 26 December 2013

1. Introduction

There are several factors contributing to the development of summer precipitation in Southeastern South America (40 °–20 °S, 45 °–65 °W, hereafter SESA), including the development of mesoscale convective systems (Velasco and Fritsch, 1987) and the passage of frontal systems (Siqueira and Machado, 2004). SESA is part of the South American Monsoon System (SAMS, Nogués-Paegle *et al.*, 2002), and is affected by the continental thermal low known as Chaco low (Seluchi and Marengo, 2000) and by its interaction with the low-level jet, which provides the moisture needed for rainfall occurrence. Both continental and ocean surface conditions may affect precipitation over SESA. Several authors have attempted to relate precipitation in the region with sea surface temperature anomalies over the Pacific, Indian and Atlantic Oceans (e.g. Cherchi *et al.*, 2013). However, interannual variability of summer precipitation in SESA appears to be less correlated with ENSO than in other seasons (Cazes-Boezio *et al.*, 2003). On the other hand, SESA has been identified as a region of strong interaction between land and atmosphere in summer (Sörensson and Menéndez, 2011, hereafter S&M11).

To understand land–atmosphere interactions, relationships between hydrological variables, as soil moisture (SM), evapotranspiration (ET) and precipitation, must be analysed. The equations of water and energy balances of the surface are connected by the ET (where ET is the latent heat flux divided by the specific latent heat). SM affects the partition of radiative energy into sensible and latent heat fluxes and, consequently, the characteristics of the boundary layer and its effect on the triggering of convection (e.g. Pielke, 2001; Taylor *et al.*, 2007). SM variability can force the atmospheric state and circulation at different time scales, from diurnal (the daily development of the planetary boundary layer) to seasonal (if SM memory is long).

The concepts of coupling, feedback, interaction and memory are commonly involved in the study of the physical processes occurring at the land–atmosphere interface. Coupling between two variables A and B is defined as the quantitative effect of one variable over the other in a one-way interaction ($A \rightarrow B$). Feedback establishes a two-way relationship ($A \leftrightarrow B$), which enhances (positive feedback)

* Correspondence to: R. C. Ruscica, CIMA (CONICET-UBA), Piso 2, Pabellón 2, Ciudad Universitaria, Int. Guiraldes 2160, Ciudad Autónoma de Buenos Aires (C1428EGA), Argentina. E-mail: ruscica@cima.fcen.uba.ar

or weakens (negative feedback) the relationship. Both coupling and feedback entail implicitly the idea of the direction of causality between two variables, whereas the concept of interaction refers to the set of relationships between two or more variables without indicating causality. On the other hand, the concept of memory involves only one variable (A) and refers to the temporal persistence of its state or anomaly, which can occasionally force the state of some other variable (B).

While some couplings between variables are obvious (e.g. Precipitation → SM), others are not easily observable because of the complexity of the interactions involved. An example is the coupling SM → Precipitation which, depending on the circumstances, may affect the intensity, frequency and persistence of the precipitation. For the coupling SM → Precipitation to be effective, a necessary (although not sufficient) condition is that the coupling SM → ET is effective as well, allowing the coupling ET → Precipitation. The coupling SM → ET requires that the soil is not too close to saturation as in that case, what limits ET is the energy required to evaporate water and not SM (e.g. see Figure 5 in Seneviratne *et al.*, 2010). Improved knowledge of the SM → ET coupling characteristics may contribute to better understand the interactions of soil with other variables (e.g. surface air temperature).

Recent studies have explored different aspects of the interaction between the continental surface and the atmosphere during austral summer in South America. Limited area atmospheric models were used to demonstrate that precipitation is sensitive to SM initial conditions in the region (Collini *et al.*, 2008; Saulo *et al.*, 2010; Sörensson *et al.*, 2010). Surface temperature anomalies and precipitation in SESA simulated by a global atmospheric model were improved when SM–atmosphere interactions were included (Barreiro and Díaz, 2011). A more detailed representation of surface processes, including vegetation biophysical processes, improves the representation of the surface fluxes, low-level circulation and precipitation of the SAMS (Ma *et al.*, 2011). Land–atmosphere interaction seems to be particularly important in SESA given the high-coupling strength (CS) between SM and ET and between SM and precipitation (S&M11 and Wang *et al.* (2007); that used different types of models and coupling metrics). The statistical analyses of the GSWP-2 database (a SM database generated by stand-alone land surface schemes forced by reanalysis and meteorological observations), suggest that the ET rate is controlled by SM rather than by the atmospheric conditions, and that the SM memory is up to 20 days for SESA in summer (Dirmeyer *et al.*, 2009).

Most of the SESA region belongs to the southern La Plata Basin (LPB), the second largest basin in South America where a large part of the population and the economic activities of the continent are located. One of the objectives of the CLARIS LPB FP7 European Project (www.claris-eu.org), in which the authors participated, was to identify the regions that are most likely to exhibit land–atmosphere interactions in the LPB. In this context, this article aims at further understanding the coupling SM → ET, the SM memory and precipitation characteristics in SESA by analysing an ensemble of simulations of the summer period December 1992–February 1993 from a regional climate model (RCM).

2. Model characteristics

The Rossby Centre Regional Atmospheric Climate Model (RCA3-E), which was developed at the Rossby Centre/Swedish Meteorological and Hydrological Institute, was used for this study (Kjellström *et al.*, 2005; Samuelsson *et al.*, 2011). The primitive equations are resolved on a rotated grid with 0.5° resolution and 24 sigma levels in the vertical, of which the 5 lowest ones are below 900 hPa. The model's geographical domain covers South America. Initial and boundary conditions (updated every 6 h) are interpolated from the ERA-40 reanalysis database (Uppala *et al.*, 2005). A review of the main characteristics of RCA3-E is found in Table 1. For more details and differences regarding previous versions, the reader can refer to Sörensson (2010). For soil temperature and soil moisture prognostic variables, the soil column is divided into five and two layers, respectively. Total soil moisture depth is equal to total rooting depth and the top soil moisture layer has a depth of 7 cm, whereas the depth of the second one is defined by the spatially variable rooting depth of ECOCLIMAP. For example, in the tropical forest of Amazonia the rooting depth reaches 8 m, meanwhile in SESA it is 1–2 m. With respect to the land surface cover, RCA employs three tiles for separate calculation of fluxes of momentum and latent and sensible heat fluxes: open land, coniferous forest and broadleaved forest. The open land tile is subdivided into a vegetated and a bare soil part, and the forest tiles include canopy and forest floor. The vegetation parameters like leaf area index (LAI), albedo, surface roughness length and rooting depth are taken from the ECOCLIMAP database (Masson *et al.* 2003), and are redefined over the three tiles mentioned. In this study, three regions in SESA were selected based on the methodology described in Section 5. The most important vegetation and soil properties of these regions are presented in the Appendix A.

3. Methodology

The CS between SM and ET (hereafter CS[SM,ET]) in the South American domain was calculated by S&M11 (see Appendix B for a description of the methodology). Coupling between SM and precipitation will only be found in regions with high CS[SM,ET] and with a high variability of ET. If the variability of ET is too low in a region with high CS[SM,ET], the SM influences on the ET, but the temporal changes of ET will be too weak to influence on precipitation. Figure 1(a) and (b) shows the CS[SM,ET] and the temporal variability of evapotranspiration σ_{ET} respectively, calculated from daily values. The product of these two indices, shown in

Table 1. Grid configuration and main parameterizations of RCA3-E.

Projection	Rotated pole
Grid resolution	0.5°
Grid size (latitude × longitude)	155 × 134
Vertical coordinate	Hybrid
Vertical levels	24
Advection	Semi-Lagrangian
Convective scheme	Kain and Fritsch (1993)
Cloud microphysics scheme	Rasch and Kristjansson (1998)
Radiation scheme	Savijärvi (1990), Sass *et al.* (1994)
Land surface scheme	Samuelsson *et al.* (2006)
Soil thermal layers	5
Soil moisture layers	2

Figure 1(c), can be thought of as a 'coupling efficiency'. The main hotspot of land–atmosphere coupling efficiency in summer over South America is found in SESA (Figure 5(b) of S&M11 shows the same product, but with a temporal scale of 6-day means, which gives approximately the same result).

In this study, an ensemble of ten 4-month continuous simulations will be analysed. The ensemble members differ in initial dates (04, 07, 10, 13, 16, 19, 21, 24, 26 and 28) of October 1992–March 31st 1993 (period with neutral ENSO conditions). In order to initialize the SM of the regional model in equilibrium with the atmosphere – without using a long spin-up time for each simulation – the 10 different SM initial conditions were set to the SM fields of the corresponding date of a RCA3-E multi-year integration, initialized on 1 September 1990.

4. Observation uncertainties and model evaluation

The mean field of seasonal rainfall in the period December 1992–February 1993 is shown in Figure 2(a). This field presents a south-north gradient and some local maxima over the northern coast of the domain and on the eastern slope of the cordillera. To evaluate simulated rainfall, the CPC-uni database (Climate Prediction Center, Chen *et al.*, 2008) which is a daily gridded database with $0.5^\circ \times 0.5^\circ$ resolution, obtained from optimal interpolation of gauge data, was used. The relative bias of RCA3-E with respect to CPC-uni is shown in Figure 2(b). RCA3-E presents biases ranging from −40% for the south of Brazil and the northwest of Argentina to 100% on the eastern slope of the cordillera, probably due to orographic effects (this is a common problem in climate models, e.g. Fernandez *et al.*, 2006; Urrutia and Vuille, 2009). Nevertheless large uncertainties in observational datasets used for validating models near and over the Andes are also evident (e.g. Negrón Juárez *et al.*, 2009; Carvalho *et al.*, 2012; McGlone and Vuille, 2012). Furthermore, RCA, as most RCMs and Global Climate Models (GCMs), has problems in representing summer precipitation over SESA (e.g. Christensen *et al.*, 2007; Carril *et al.*, 2012, Solman *et al.*, 2013).

To put these model errors into a context and as a measure of its uncertainty, a crude measure of the observational uncertainty was defined as the difference between two databases: CPC-uni and the CRU monthly database (Climatic Research Unit, New *et al.*, 1999, 2000). The relative percentage difference between CRU and CPC-uni databases is shown in Figure 2(c). The relative difference between the two databases (Figure 2(c)) and the relative model bias (Figure 2(b)) is similar in sign, location and magnitude in several regions, except the northwestern slope of the Andes, where the model overestimates the values of both databases. The uncertainty in the observations over a great part of SESA does not allow quantifying the model error in representing the mean rainfall of the austral summer 1992–1993.

The rainfall frequency (number of days with rain above 1 mm) is shown in Figure 3(a). Frequency is interesting in the context of the analysis of the coupling between SM and the atmosphere because SM may play a role in triggering convective rain. Humid soils reduce the Bowen Ratio (ratio between sensible and latent heat flux), favouring the flux of energy from the soil and convective instability (e.g. Eltahir, 1998; Alfieri *et al.*, 2008; Jaeger and Seneviratne, 2011). In general, the areas with the greatest rainfall occurrence coincide with those with the highest mean (see Figure 2(a)), i.e. the south-north gradient pattern is still observable, although the local maximum over the northwestern slope of the Andes is less evident for frequency than for mean rainfall. The spatial pattern of the relative bias of the number of days with rainfall in RCA3-E with respect to CPC-uni (Figure 3(b)) is similar to the spatial pattern of the relative bias of mean precipitation (Figure 2(b)). Frequency is underestimated in the east of SESA, which coincides partially with the negative bias of the mean. However, there are some areas where the bias has different sign (for instance the southeastern coast of Brazil). It is worth noting that Figure 3(b) does not agree with previous results over the region (e.g. Carril *et al.*, 2012), where the frequency of rainy days is overestimated. Beyond existing model errors, as the underestimation of strong precipitation (a common problem in most RCMs), the pattern in Figure 3(b) could be related to the overestimation of the frequency of days with low precipitation in the CPC-uni database as suggested in Carvalho *et al.*, 2012 (e.g. percentile 25 of daily precipitation for this data set is the lowest in an intercomparison of observational precipitation datasets over South America).

Figure 4(a) shows the Mean daily Intensity of Precipitation (hereafter MIP) defined as the total seasonal precipitation divided by the number of days with rainfall above 1 mm. MIP maxima are located where extreme rainfall events (identified for instance by the 95th percentile, not shown) take place. Therefore, MIP is a good metric of daily rainfall extremes.

Further information on the capabilities of this model to simulate different precipitation features in the region can

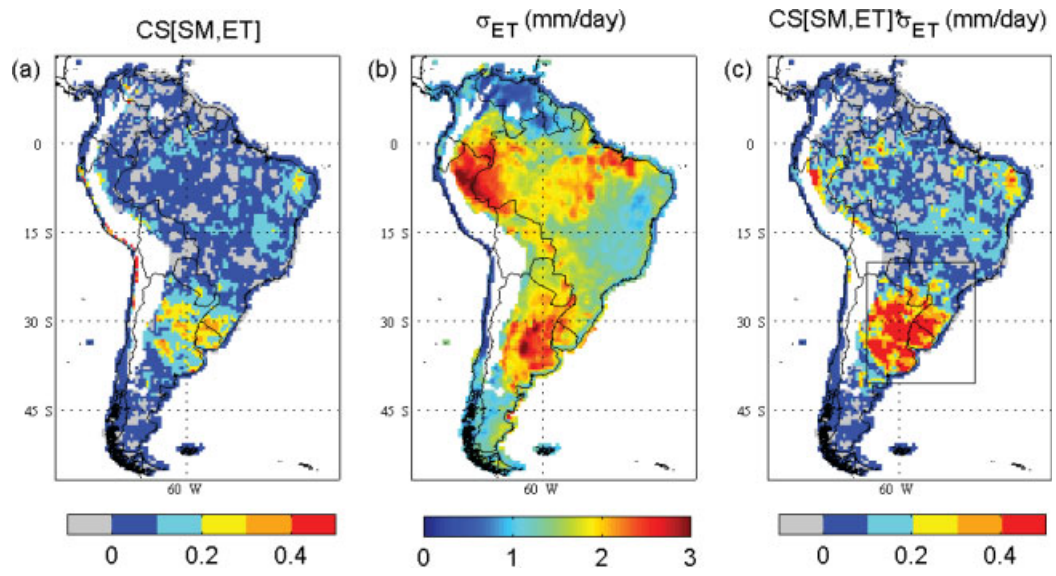

Figure 1. (a) Coupling strength CS[SM,ET], (b) standard deviation of evapotranspiration (σET, mm day^{-1}) and (c) coupling efficiency, defined as the product CS[SM,ET]* σET, which is similar to Figure 5(b) of S&M11, but on a daily time scale. The box indicates the studied region (SESA). Ocean as well as terrain higher than 1200 m are masked.

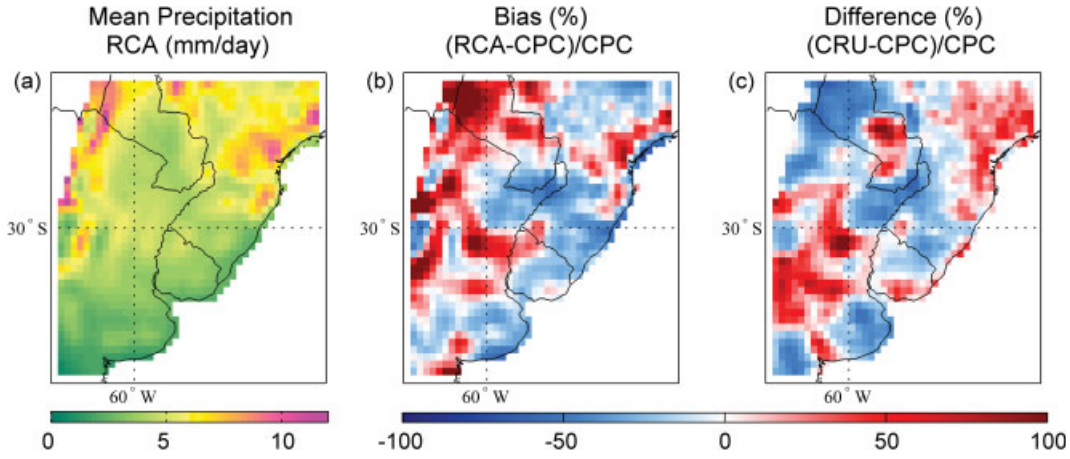

Figure 2. Mean summer precipitation. (a) Model (mm day^{-1}). (b) Relative bias (RCA-CPC)/CPC (%). (c) Difference between CRU and CPC data (CRU-CPC)/CPC (%).

be found in Menéndez *et al.* (2010a, 2010b) and Carril *et al.* (2012).

5. Evapotranspiration forcing

Three subregions (R1, R2 and R3) were defined based on MIP (Figure 4(a)) and CS[SM,ET]*σ_{ET} (Figure 4(b)) in SESA, in order to improve the understanding of the physical mechanisms involved in areas of coupling/no coupling efficiency and high/low rainfall intensity. Here, all points with CS[SM,ET]*$\sigma_{ET} < 0.2$ are considered to have no coupling efficiency, and points with CS[SM,ET]*$\sigma_{ET} \geq 0.2$ are considered as points with coupling efficiency. The limits for MIP are the first and last quartiles including all points in the SESA domain except for oceans and grid points with altitudes above 1200 m (Table 2). The subregions were defined inside boxes of equal size (Figure 4(c)). The subregion R1 is characterized by no coupling efficiency and high MIP, R2 by coupling efficiency and high MIP and R3 by coupling efficiency and low MIP.

To understand the physical mechanisms involved, spatial averages of different variables were calculated for each day and member of the ensemble, which yields 90×10 values for each region. The horizontal axis in Figure 5(a)–(c) represents the seasonal evolution of the logarithm of daily rainfall, and each row on the vertical axis represents a member of the ensemble. The differences among rows make it possible to estimate the internal variability of each region. The lowest variability occurs when there is coincidence between rows, as for instance in R2 during the last 20 days (see Figure 5(b)) where rainfall is less than 1 mm day^{-1} in all the members of the ensemble.

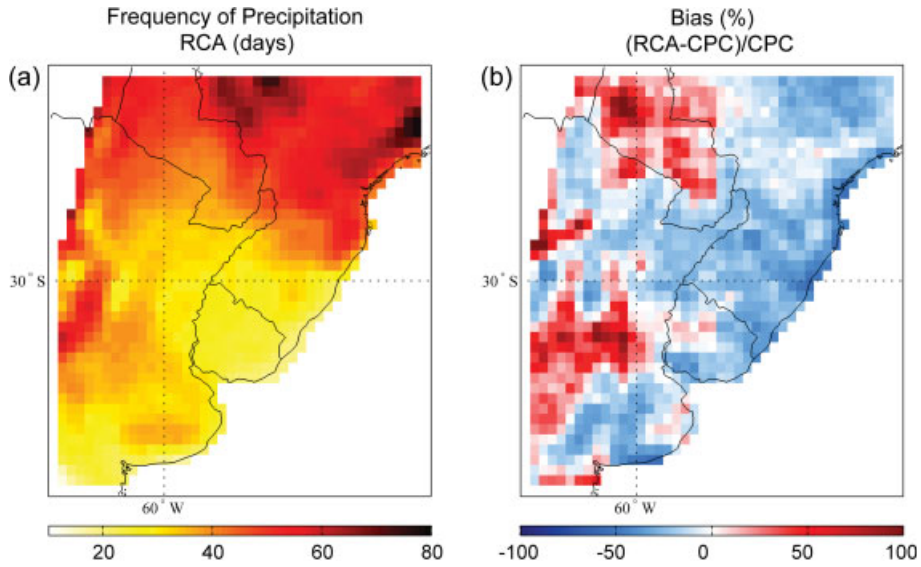

Figure 3. Frequency of occurrence of precipitation greater than 1 mm. (a) Model (days). (b) Relative bias (RCA-CPC)/CPC (%).

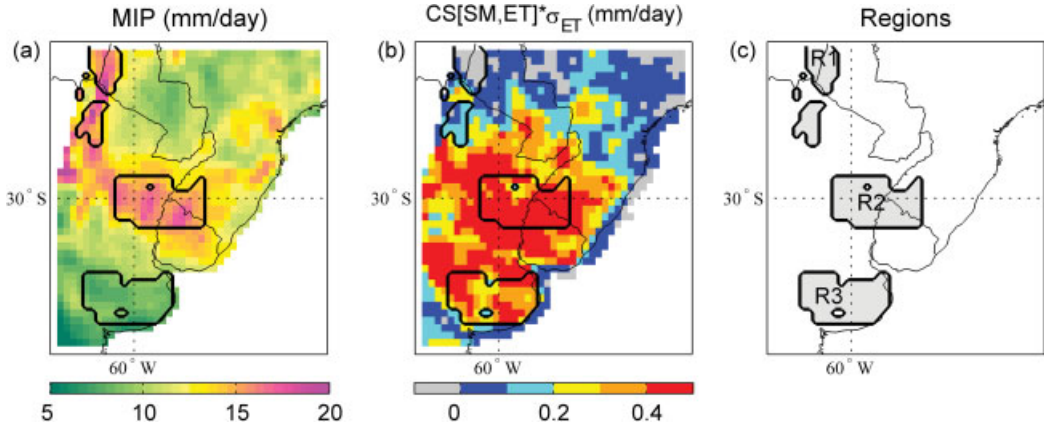

Figure 4. (a) Mean daily Intensity of Precipitation (MIP, mm day^{-1}). (b) Coupling efficiency (mm day^{-1}, box in Figure 1). (c) Subregions analysed in this study, as determined using Figure 4(a) and (b) along with the criteria of Table 2 (see text).

Table 2. Criteria to define subregions in SESA (based on Figure 4(a) and (b)).

	R1	R2	R3
CS[SM,ET]*σ_{ET}	<0.2	>0.2	>0.2
MIP	>percentile 75	>percentile 75	<percentile 25

To examine whether these characteristics reflect on surface variables, scatter plots (Figure 5(d)–(f)) were built with the 900-data series of mean areal ET and soil water availability (SWA). SWA is calculated as a function of both SM soil layers, and is a measure of the degree of saturation. SWA values range from 0 (permanent wilting point) to 1 (field capacity). Light and dark grey indicate mean areal precipitation exceeding the 75th and 95th percentile respectively, i.e. extreme events of precipitation. Mean seasonal values of SWA and ET are shown with vertical and horizontal lines. Note that mean SWA also contains information from a time prior to the study period, because of the spin up of the simulations.

In R1 (region with no coupling and high rainfall intensity), the absence of coupling efficiency is already a sufficient condition for the absence of feedback SM $\leftrightarrow$ Precipitation through ET. It is worthwhile to describe some of the mechanisms involved in order to understand whether the lack of coupling is related with heavy rainfall represented by high MIPs. The comparison of subregions in Figure 5(a)–(c) reveals that intense rainfall events are more frequent in R1 than in R2 and R3 (behaviour already displayed in Figure 4(a)). Variability among members is also greater in R1, as in the first 15 days of the season. For example, in R1 on day 13 the difference among members is as much as 26 mm whereas the mean is only 4 mm. Mean SWA is also higher in R1 than in the other two regions (Figure 5(d)–(f)) which is a consequence of the rainfall characteristics.

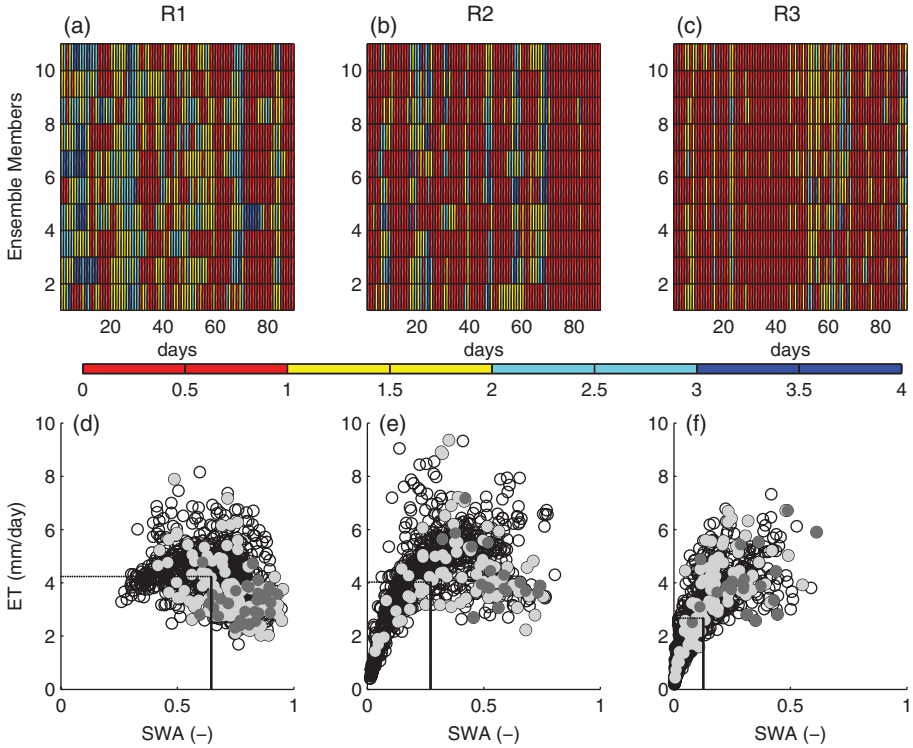

Figure 5. Top panel: Seasonal evolution of mean areal of the logarithm of daily precipitation for each ensemble member in subregions R1 (a), R2 (b) and R3 (c). Bottom panel: Scatter plots of daily mean areal of ET and SWA, in subregions R1 (d), R2 (e) and R3 (f). Cases where rainfall is higher than percentiles 75 and 95 are marked in light and dark grey, respectively. The average values are indicated by vertical and horizontal lines.

The functional relationship observed between SWA and ET is determined by its physical and meteorological conditions and with the soil type and vegetation cover. When soil and vegetation are able to supply water without limitations (i.e. conditions close to field capacity), the local atmospheric conditions (e.g. temperature) control the latent heat flux from the surface, i.e. evapotranspiration. This type of interaction is likely to appear in R1 (Figure 5(d)), where the mean SWA is 0.64. High SWA values are associated with the lowest ET values in the region, and they often occur under extreme precipitation (dark grey points). In such cases, the atmosphere is very moist and incoming radiation is limited by cloudiness and hence the amount of water that can evaporate from the surface decreases. In addition, the mean, frequency and intensity of precipitation in the region are high (see Figures 2(a), 3(a) and 5(a)). The atmospheric moisture in R1 has a large contribution from the Amazon rainforest, i.e. a large component origins from non-local sources. With respect to local sources it is worth mentioning that, for equal atmospheric conditions of temperature and relative humidity, the vegetation of R1 has a higher capacity of evapotranspiration compared to R2 and R3. This can be qualitatively estimated from the Table A1 in Appendix A, the parameters surface roughness (z0), rooting depth and LAI are higher in R1 than in R2 and R3. LAI and z0 increases evapotranspiration through lower surface and aerodynamic resistance to latent heat flux. The rooting depth is equal to the soil depth in RCA (Section 2) and determines the total water storage capacity, and decreases the possibility of water depletion. In comparison with the two other regions, R1 also has a slightly lower albedo, which increases the total energy available for surface fluxes. It is difficult to estimate the contribution from non-local and local sources to the atmospheric moisture of R1, but from Figure 5(d) it is clear that atmospheric conditions determine the behaviour of ET in R1; reducing the potential effects of soil on ET and consequently on precipitation.

Regions of coupling efficiency (in this case R2 and R3, see Figure 4(b) and (c)) meet the necessary, although not sufficient, condition for the existence of feedbacks. In such regions, more or less intense rainfall (over R2 and R3, respectively) might be triggered or enhanced by surface coupling, beyond the usually dominating large-scale atmospheric circulation processes. The distribution of points in the scatter plot for R2 (Figure 5(e)) is quite different from that of R1. High values of CS[SM,ET] in the region are coherent with the positive correlation between SM and ET, given that CS is a measure of the degree of variance of ET that is explained by the boundary conditions, in this case, by SM (see the Appendix B). Although mean ET is similar to that of R1, the range of ET values is larger which is consistent with the high value of the diurnal variability factor σ_{ET} in the region. The figure shows a quasi-monotonically increasing relationship between the variables which determines that ET

is limited by SWA. The relationship between the variables is almost linear until SWA values are close to the mean (0.27), and it becomes more scattered above that value. The distribution of the light and dark grey points shows that ET is less dependent on SWA during extreme precipitation events, possibly because cloudiness and atmospheric moisture near the surface are higher.

R3 (region with coupling and low rainfall intensity) is the driest region, and has the highest number of days with precipitation below 1 mm (Figure 5(c)). Large values of CS[SM,ET]*σ_{ET} in this subregion denote that ET is also controlled by SWA and Figure 5(f) is similar to Figure 5(e). On the other hand, a lower MIP in R3 reflects in lower mean SWA and consequently lower mean ET as well. The distribution of points in Figure 5(f) suggests a more defined functional relationship between SWA and ET in R3 (data are less scattered in R3 than in R2).

Regarding land surface cover parameters (Table A1, Appendix A), these are similar for R2 and R3. The z0 and rooting depth, which influence positively on the evapotranspiration capacity, are slightly higher in R2 than in R3. On the other hand the LAI, also increasing the evapotranspiration capacity, is higher in R3 and the albedo, which decreases the total surface fluxes is higher in R2. Therefore, estimations of how the land surface cover could influence on differences in the behavior of the evapotranspiration of these two regions are difficult to make.

6. Correlations between land surface variables

A way of quantifying the degree of the relationship between the variables showed in the scatter plots is through correlations. Spearman's correlation is a more robust alternative to Pearson's traditional linear correlation, as it allows quantifying the relationship between the variables with no need of assuming linearity (Wilks, 2006). Unlike Pearson's correlation, Spearman's correlation is applied on ranked variables (data are replaced by their position in the ascending order of the values). Table 3 shows the correlations of different combinations of daily ET, PP (precipitation), T (temperature at 2 m) and top and root-zone SM for the three subregions. The correlations are calculated for each grid point and those that are significant at 99% (two-tailed Student's test, correlations significant at 95% are almost equal) are averaged over each region. One-day lag autocorrelations of SM and PP are shown (marked with +).

In the table, the first column quantifies the strength of the relationships analysed in the scatter plots of the previous section (Figure 5(d)–(f)) besides the variable is SM instead of SWA. When ET is controlled by the atmosphere (as in R1) the correlation coefficient r(SM,ET) is negative, whereas a positive correlation (as in R2 and R3) indicate that ET is controlled by SM. The coefficient r(SM,ET) for root-zone SM in R1 is negative although almost zero, which indicates that the daily influence of ET on root-zone layer SM is not important. R2 has the same correlation coefficients for both layers, which indicates that ET is equally related to top and root-zone SM. In R3, ET correlates somewhat less with root-zone SM than with top SM. Values in the second column, r(ET,T), can be seen as complementary of those in the first column, and are therefore opposite in sign. In R1, higher temperatures increase the water holding capacity of the air, and ET increases. In R2 and R3, higher SM implies a decreased Bowen ratio through higher ET and consequently lower sensible heat flux and lower temperatures. The signs of r(ET,PP) (3rd column) and r(SM,ET) for each region are equal. In R1, as discussed before, the correlation of ET with precipitation is similar to its correlation with SM, whereas in R2 and R3, r(SM,ET) is greater than r(ET,PP). The correlation between top SM and precipitation is similar among the subregions (4th column). The one-day lag autocorrelation of SM (5th column) is high in all subregions. Correlation values are greater in the root-zone layer than in surface layer, because the temporal evolution of the variables in underground layers is slower. On the other hand, the autocorrelation of precipitation (last column) is weaker than that of SM, which is consistent with the fact that SM is a more persistent variable than precipitation (see Section 6 below). A weak south-north gradient is observed from R3 to R1 in SM autocorrelations in both soil layers. On the other hand, the spatial gradient of precipitation persistence is more marked. This gradient was also observed in the mean and frequency of precipitation (see Section 3, Figures 2(a) and 3(a)).

7. Soil moisture memory

SM data may improve monthly to seasonal precipitation predictions in some regions and seasons, given that through ET, long SM memory can affect the state of the atmosphere. For this to happen, SM memory and scale of prediction have to be equal and the coupling efficiency

Table 3. Areal average of daily correlations significant at 99%.

Correlations	r(SM,ET)	r(ET,T)	r(ET,PP)	r(SM,PP)	r(SM,SM+)	r(PP,PP+)
R1	−0.29 (−0.02)	0.38	−0.32	0.59(0.16)	0.88 (0.99)	0.63
R2	0.61 (0.61)	−0.42	0.12	0.52(−)	0.85 (0.97)	0.56
R3	0.78 (0.70)	−0.26	0.19	0.43(0.12)	0.82 (0.96)	0.31

Values for root-zone layer soil moisture are shown in parentheses. The + sign indicates lag 1. (−) means that there is no significant value at 99%.

has to be strong enough, i.e. SM has to leave a signal in the atmosphere.

According to Koster and Suarez (2001), SM persistence is controlled by different physical drivers such as ET, runoff, the temporal correlation between SM and atmospheric forcing (e.g. rainfall or net radiation) and the temporal variability of the atmospheric forcing. While the first two are intuitive, the third one is understood, e.g. as the influence of rainfall persistence on SM memory. The persistence of rainfall is less than that of SM because the characteristic time scale of atmospheric dynamics is smaller (Dirmeyer *et al.*, 2009). The factors able to enhance or weaken persistence are internal atmospheric dynamics, the memory of some external forcing (e.g. sea surface temperature) or the continental surface memory through feedbacks. In areas of higher precipitation persistence, the land surface states are more sustained (Wei and Dirmeyer, 2010). Those areas may tend to states of equilibrium such as very humid or arid soils, which cancel soil–atmosphere feedbacks.

Mathematically, persistence can be estimated as a positive statistical dependence among successive values of the same variable. For continuous variables (such as temperature or SM), persistence can be characterized in terms of serial correlation or temporal autocorrelation (Wilks, 2006, Section 3.5.4).

Studying the persistence of SM implies studying the persistence of precipitation, given that precipitation is one of the main forcing for SM. As precipitation is a discrete variable, its persistence (in its statistical meaning) is given by the conditional probability of precipitation occurrence/non-occurrence (Wilks, 2006, Section 2.4.4). A non-statistical method to estimate precipitation persistence is the average of consecutive days with precipitation above a given threshold. Figure 6 shows such metric for a threshold of $1\,\mathrm{mm\,day^{-1}}$, where a gradient with approximately south–north direction can be observed, similar to the gradients observed for the mean and frequency (Figures 2(a) and 3(a)). At some grid points in the northeast of SESA, the mean duration of rainfall events are up to 6 days. Regions with high rainfall persistence (including R1) are humid and coincide with the regions with low CS[SM,ET]*σ_{ET} (Figure 4(b)).

SM memory can be defined as the time (in days) required for the autocorrelation of SM to drop below the 99% confidence level (Dirmeyer *et al.*, 2009). This provides an estimate of the number of days during which the SM trend remains more or less invariable. Although calculations can be made for the complete 90-day period it is statistically correct to determine the maximum lag at about 30–40% of the number of data. In our case, we have set 30 days as the maximum value. The lowest significant autocorrelation value defines the memory for each grid point.

Figure 7 shows the autocorrelation functions of daily SM at the top and root-zone layers for all the grid points in each of the three subregions. The maximum statistically significant memory is restricted to 30 days

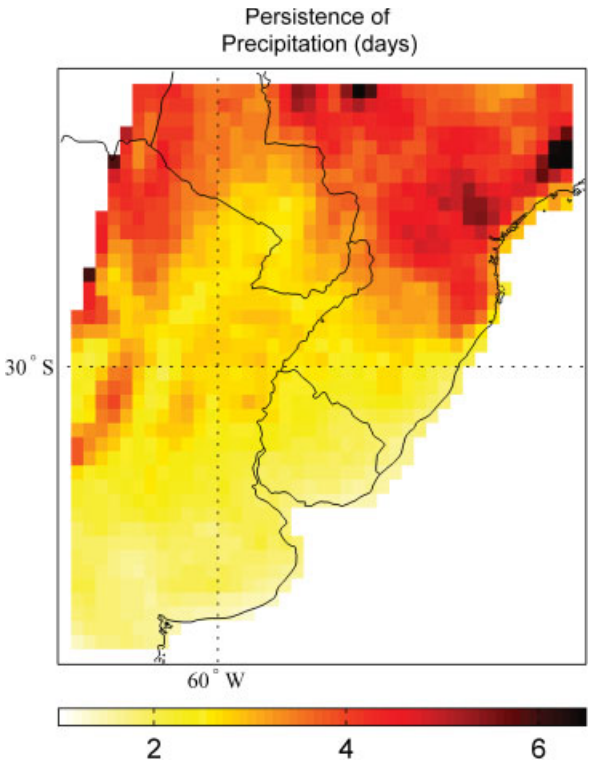

Figure 6. Persistence of precipitation ≥1 mm (days, see text for details).

(1/3 of the amount of available data). The average memory for each subregion is defined by the average of the memory at all grid points. The figure shows the difference of SM persistence (1) between soil layers and (2) among subregions. With regard to (1), in any of the three subregions, the autocorrelation of SM in the root-zone layer decreases at a lower rate than on the surface because of the time scale of the variability characteristic to each layer. Consequently, the memory is longer at greater depth. As to (2), R1 has the longest memory. R1 is also the least homogeneous, given that the spread among autocorrelation curves is high relative to the other subregions, possibly due to the high spatial variability of precipitation.

The differences in shape of the autocorrelation curves in the three subregions can be explained by the drivers described by Koster and Suarez (2001). The drivers acting in R1 are different from those acting in R2 and R3, as the time scale at which the autocorrelation is no longer significant is greater. In R1, the autocorrelation values are always significant at 99% in 30% of the total amount of grid points in the case of the top layer and 16% in the case of the root-zone layer. Those points have a 30-day memory at 99% significance. In the root-zone layer in R1 (Figure 7(d)), the autocorrelation curve is quasi-monotonically decreasing, whereas the curve for the top layer (Figure 7(a)) tends to oscillate around a certain value after day 10. In particular, two groups of curves are observed oscillating around 0.4 and 0.2 approximately. This makes it possible to infer that top SM is forced by the periodic autocorrelation of some external factor (e.g.

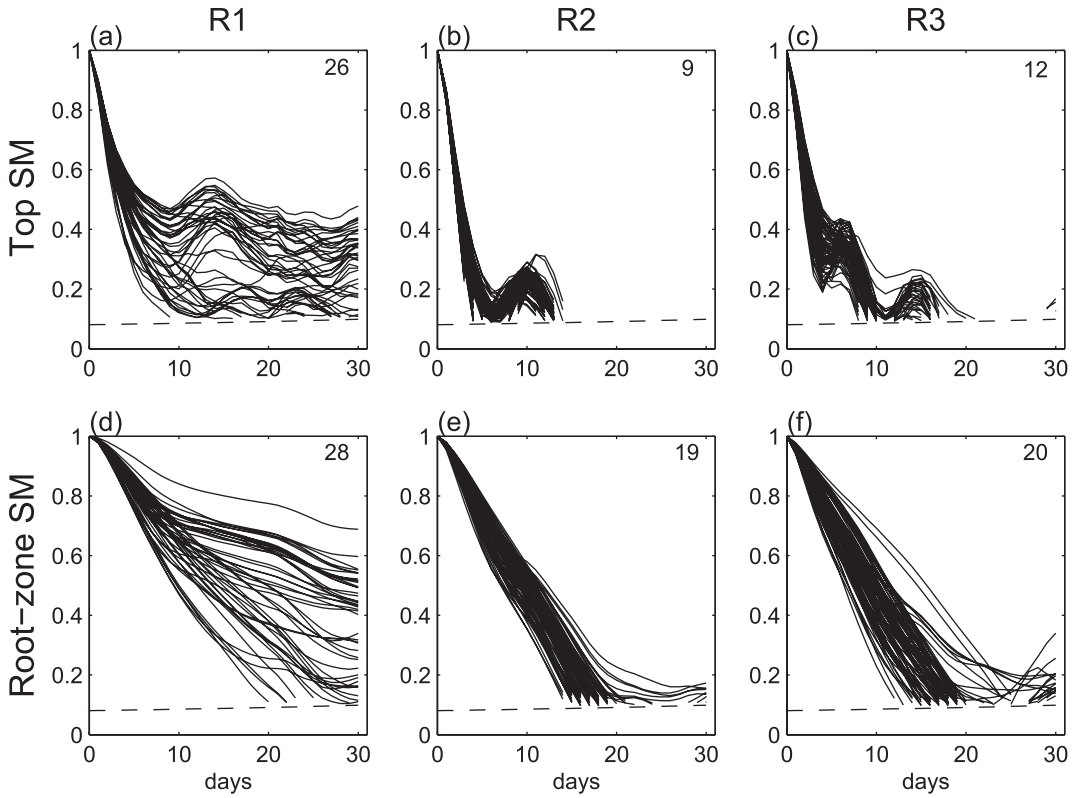

Figure 7. Autocorrelation functions of soil moisture for each grid point in the three subregions (R1 left, R2 centre, R3 right) and layers (top: surface layer, bottom: root-zone layer). The statistical significance at 99% is shown (dotted line) and the numbers in the upper right corner indicate the average memory.

precipitation and/or radiation). Therefore, R1 is a region with two different top SM memories. These two regimes are less distinguishable in the root-zone layer.

The results of R2 and R3 are similar. However, one difference between R2 and R3 is the region's homogeneity (less spread in R2). At some grid points, the curves decrease monotonically up to the statistical significance, indicating that at those points external forcing(s) is (are) not enough to affect the trend of SM, thus the memory value is not 'contaminated'. On the other hand, all the grid points in R3 are affected by external drivers (Figure 7(c)), as the first minimum in autocorrelation (around day 5) appears before the mean memory value (day 12). Because of this, the mean surface memory in R3 (12 days) is slightly longer than in R2 (9 days).

Figure 8 shows the memory of SM for the top and root-zone layers. The values correspond to the days when the autocorrelation function crosses the significance curve (see Figure 7). As mentioned before, high autocorrelation values of SM might be related to areas of highly persistent rainfall (some points in R1) or to a regime of low ET or low runoff. In the case of top SM (Figure 8(a)) a minimum memory (0–5 days) is located over the north of Uruguay, south of Brazil and some points in Argentina and Paraguay. In this area, the 5 to 6-day lagged correlation between SM and subsequent precipitation was found significant (not shown), which indicates that the third driver of Koster and Suarez (2001), i.e. the temporal correlation SM–atmospheric forcing, appears in this region. High memory values in the northwest (30 days) are consistent with high rainfall persistence (see Figure 6), and with the characteristics of high MIP and low CS[SM,ET]*σ_{ET} (see Figure 4(a) and (b)).

As could be expected, SM memory (Figure 8(b)) in the root-zone layer is longer than in the top layer. The comparison of this figure with Figure 4(b) reveals that minimum memory (lighter colours) are located approximately in the region of high CS[SM,ET]*σ_{ET}, except for a smaller region in the northeast of SESA. Thus, the region of maximum CS[SM,ET]*σ_{ET} coincides approximately with a minimum of SM memory in the root-zone layer, with memory values between 10 and 30 days. In most of the areas where CS[SM,ET]*σ_{ET} is low (north and southwestern corner of SESA) the memory of the root-zone layer is long. This is because when changes in SM are slow (long memory), there is little influence from the soil to the atmosphere and the fraction of atmospheric variability that depends on SM (CS) is low. According to these results, the coupling efficiency would be inversely related to the longest memory of the system, i.e. that of the deepest layer. However, there are areas with strong coupling efficiency in Uruguay and parts of eastern Argentina where the root-zone SM memory is around 30 days.

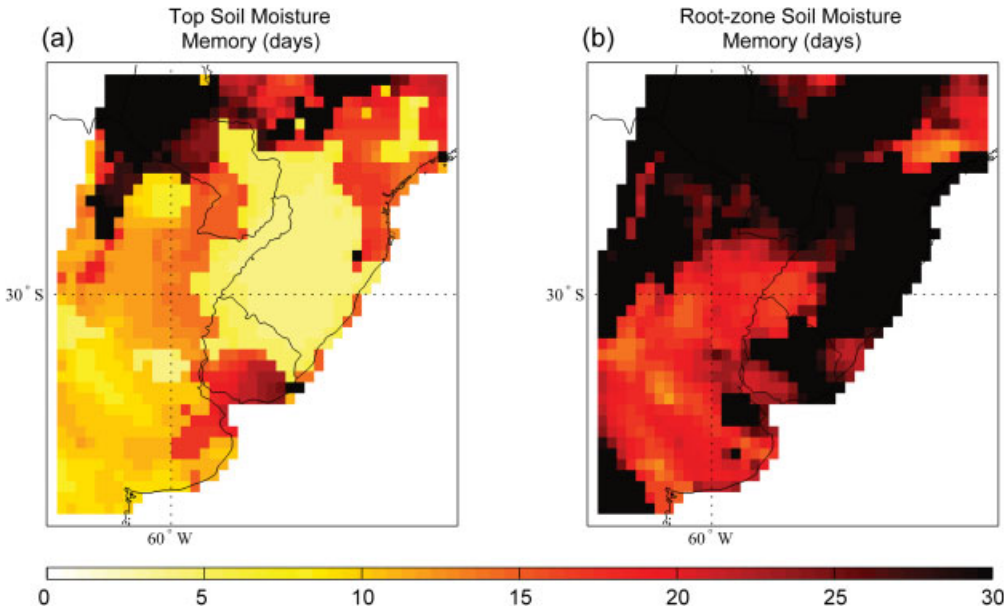

Figure 8. Soil moisture memory (days) for the (a) surface layer and (b) root-zone layer. Memory is defined as the lag for which the autocorrelation value is significantly lower than 99% (see Figure 7). The darker colour indicates that the memory is up to 30 days with a 99% significance level.

8. Conclusions

Results from previous studies suggest that the SESA region presents a hot spot between soil moisture and evapotranspiration (e.g. S&M11). The aim of this study was to further understand some of the processes involved in land–atmosphere interaction in different subregions of SESA. In areas with coupling efficiency and high MIP (as in R2), the correlation between soil moisture and evapotranspiration, r(SM,ET), is positive and high for both top and root-zone SM, indicating that both layers interact with the atmosphere through ET. In areas with coupling efficiency and low MIP (as in R3), the top soil layer interacts more with the atmosphere than the root-zone layer. It is difficult to qualitatively estimate the difference in evapotranspiration capacity of R2 and R3 as z0 and rooting depth are larger in R2 and LAI is larger in R3.

In areas with no coupling and high MIP (as in R1), the same correlations are negative, as higher ET implies less SM, but the correlation is very low for the root-zone layer, indicating that the daily influence of ET on root-zone layer SM is not significant. Non-local moisture sources (e.g. humidity advected from tropical latitudes) add a large part of the atmospheric humidity in this region. With respect to local sources, R1 has a larger fraction of forest than R2 and R3, and the parameters that influence positively in evapotranspiration capacity (z0, rooting depth and LAI) are consistently higher in R1. However, in this study the contribution of non-local and local ET is not analysed. The correlation r(ET,T) is a measure of the interaction between soil and temperature through ET. Subregions with coupling efficiency (as R2 and R3) have negative r(ET,T), which indicates that ET controls temperature (evaporative cooling), whereas the positive correlation in areas with no coupling (as R1) confirms that ET is controlled by atmospheric conditions (temperature, radiation, vapour pressure deficit).

The use of more realistic SM conditions for initializing meteorological forecast models may contribute to increase the predictability of atmospheric conditions. This requires a strong land–atmosphere coupling as well as a memory of soil states of at least the same time scale as the scale of the prediction. SM memory was estimated for both model layers: the top layer (0–7 cm) and the root-zone layer. The high persistence, frequency and intensity of simulated precipitation in R1 induce high SM values which remain throughout the simulation. In this sense, the memory in this region is long. In subregions of SESA where the coupling efficiency is strong (R2 and R3) the memory is shorter, and the relatively moisture region (R2) has a somewhat shorter average memory than the drier region (R3). Other features are that the memory is longer in the root-zone layer than in the top layer, and that the dispersion among SM autocorrelation curves at different grid points is largest in R1 and smallest in R2. A comparison of the memory maps reveals that the memory spatial pattern is considerably distinct for the two soil layers over vast areas of the domain (e.g. the south of Brazil). In the root-zone layer, the memory is in general anticorrelated with the coupling efficiency, as when changes in SM are slow (long memory) there is little influence from the soil to the atmosphere. Consequently, the fraction of atmospheric variability that depends on SM (i.e. CS) is low. However, Uruguay and parts of eastern Argentina have both strong coupling efficiency and SM memory around 30 days. In these last areas where an improvement of SM initial conditions could improve predictability of near surface variables on the monthly timescale. It is also worth noting that coupling

between SM and precipitation near that area (30 °–35 °S and 55 °–60 °W approximately) is strong (S&M11).

Uncertainty of memory estimates is large. Dirmeyer *et al.* (2009) computed the memory of the root-zone layer SM using two databases (GSWP-2 and GOLD-2) generated with stand-alone land surface schemes forced with reanalyses and meteorological observations. The memory values those authors obtained for austral summer in SESA is up to 20 days (GSWP-2) and from 15 to 55 days (GOLD-2). Our results are in agreement with those ranges for this region and season: memory in the range of 15–25 days for central Argentina and longer for surrounding areas. It should be pointed out that one must be cautious about these results as they are valid for only one model and one summer.

Vegetation can influence precipitation and, therefore, soil–atmosphere coupling and persistence of soil moisture. Two mechanisms linking vegetation and precipitation have recently been proposed. Their implications should be considered for South America due to the high percentage of land covered by forest and the intensity of the hydrological cycle on this continent: (1) Air exposure to forest cover influences subsequent rainfall (air that has passed over forests in the preceding few days produces more rain than air that has passed over little vegetation as a result of a higher air moisture content resulting from forest evapotranspiration, Spracklen *et al.*, 2012). This mechanism could influence principally on regions receiving northern flow from areas with relatively extensive vegetation (as subregions R1 and R2 that receive flow from tropical South America). (2) Evapotranspiration and subsequent condensation of water vapour are associated with a decline in air pressure in the lower atmosphere and therefore has an impact on atmospheric dynamics (Makarieva and Gorshkov, 2007; Makarieva *et al.*, 2013). This effect could be important on the Amazon Basin, but the further south regions analysed in this article are relatively little forested.

Model biases affect their representation of real coupling and memory. Given the observational uncertainty in South America, estimating biases is challenging, but an exception is region R1 which has a moist bias (associated with the forced lifting of air masses over the foothills of the Andes) regardless which observational database (CRU or CPC-uni) is compared with the model. However in this study the model is used as a physical framework for studying soil moisture–atmosphere interactions, and does not necessarily claim a correct representation of reality.

Acknowledgements

We acknowledge the European Community's Seventh Framework Programme (CLARIS-LPB, Grant Agreement No 212492) and project PIP 112-200801-01788 (CONICET, Argentina).

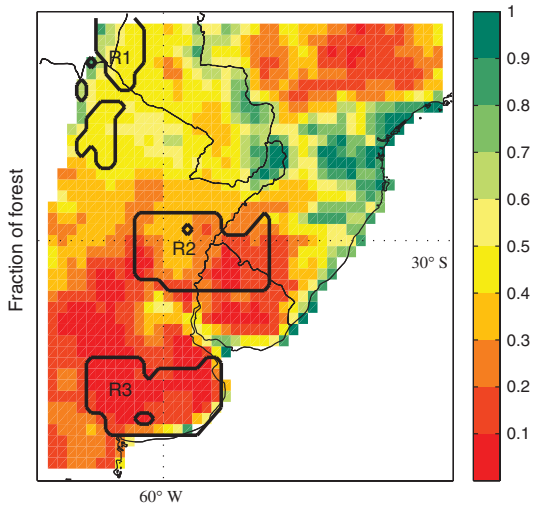

Figure A1. Fraction of forest for SESA. Regions analysed in this study are marked with black lines.

Appendix A

The three regions of study differ somewhat in soil types and vegetation cover. With respect to the first mentioned, the land surface scheme of RCA uses seven types of soil: sand, loam, clay, sandy loam, silt loam, sandy clay and peat (Samuelsson *et al.* 2011). Although the composition of soil classes is not exactly the same among the three regions, for this type of land surface scheme, the evapotranspiration depends on the wilting point and field capacity, parameters that are essentially equal.

Table A1 specifies the most important characteristics of the land surface cover: fraction of open land/forest, albedo, roughness length (z0), rooting depth and leaf area index (LAI). In the case of albedo and LAI, which vary during the year, the seasonal mean for DJF is presented.

Figure A1 complements Table A1 with a map of the fraction of forest over the studied area (regions marked with black lines). It can be seen that R3 and R2 is covered by mostly open land meanwhile R1 is half open land and half forest.

Table A1. Mean values of surface parameters of the three regions.

	Fraction open land/forest	Albedo	z0 (m)	Rooting depth (m)	LAI
R1	0.47/0.53	0.16	1.15	2.05	3.09
R2	0.79/0.21	0.18	0.32	1.39	2.52
R3	0.85/0.15	0.17	0.17	1.28	2.65

Appendix B

Two methodologies for analysing the coupling strength between soil moisture (SM), evapotranspiration (ET) and precipitation were employed by S&M11. In particular,

they calculated the coupling strength similar to Koster *et al.* (2006), called CS[SM,ET] in this work. Two ensembles of 10 members each, ensembles W and S (ensemble W was employed for this study), were created, starting from different initial dates. Ensemble S is similar to ensemble W, except that all ensemble members were forced, at each time step, to maintain the same space–time varying series of SM. Consequently, between the SM and other components of the system, and in particular the water budget, there is only a one-way interaction. The SM influences on variables like precipitation, ET and surface temperature, but these variables do not feed back upon soil moisture.

As the initial dates and the lateral boundary forcing as well as the sea surface temperature are the same for the two ensembles, the only difference between ensemble W and S is that in W, there is full interaction between SM and the atmosphere, whereas in S, the SM is a boundary condition, e.g. a day of heavy precipitation will not increase the soil water content.

The similarity (Ω_x) is then defined as the relative contribution of all boundary conditions on the variability of some atmospheric field (e.g. precipitation). The Ω_x index for any atmospheric variable x is:

$$\Omega_x = \frac{m\,\sigma_{x^\wedge}^2 - \sigma_x^2}{(m-1)\,\sigma_x^2} \tag{A1}$$

where $\sigma_{x^\wedge}^2$ is the variance of the mean time series of all members of one ensemble, σ_x^2 is the ensemble inter-member variance which is obtained by calculating the variance among all time steps and ensemble members and m is the number of ensemble members. Ω_x is interpreted as the fraction of the variance of x that is explained by boundary conditions (the total variance depends on internal variability of the model and on boundary conditions). The CS ($\Delta\Omega_{\underline{x}}$) between SM and x is defined as the difference between the similarities of the two ensembles:

$$\mathrm{CS} = \Delta\Omega_x = \Omega_x\,(S) - \Omega_x\,(W) \tag{A2}$$

$\Delta\Omega_{\mathrm{x}}$ isolates the soil moisture boundary condition which influence on the phase, amplitude and mean value of the variable x.

References

Alfieri L, Claps P, D'Odorico P, Laio F, Over TM. 2008. An analysis of the soil moisture feedback on convective and stratiform precipitation. *J. Hydrometeorol.* **9**: 280–291, DOI: 10.1175/2007jhm863.1.

Barreiro M, Díaz N. 2011. Land–atmosphere coupling in El Niño influence over South America. *Atmos. Sci. Lett.* **12**: 351–355, DOI: 10.1002/asl.348.

Carril AF, Menéndez CG, Remedio ARC, Robledo F, Sörensson A, Tencer B, Boulanger JP, de Castro M, Jacob D, Le Treut H, Li LZX, Penalba O, Pfeifer S, Rusticucci M, Salio P, Samuelsson P, Sanchez E, Zaninelli P. 2012. Performance of a multi-RCM ensemble for South Eastern South America. *Clim. Dyn.* **39**(12): 2747–2768, DOI: 10.1007/s00704-009-0165-2.

Carvalho LMV, Jones C, Posadas A, Quiroz R, Bookhagen B, Liebmann B. 2012. Precipitation characteristics of the South American monsoon system derived from multiple datasets. *J. Clim.* **25**: 4600–4620, DOI: 10.1175/JCLI-D-11-00335.1.

Cazes-Boezio G, Robertson AW, Mechoso CR. 2003. Seasonal dependence of ENSO teleconnections over South America and relationships with precipitation in Uruguay. *J. Clim.* **16**: 1159–1176, DOI: 10.1175/1520-0442(2003)16<1159:SDOETO>2.0.CO;2.

Chen M, Shi W, Xie P, Silva VBS, Kousky VE, Higgins RW, Janowiak JE. 2008. Assessing objective techniques for gauge-based analyses of global daily precipitation. *J. Geophys. Res. D: Atmos.* **113**, DOI: 10.1029/2007jd009132.

Cherchi A, Carril AF, Menéndez CG, Zamboni L. 2013. La Plata Basin precipitation variability in spring: role of remote SST forcing as simulated by GCM experiments. *Clim. Dyn.* **1–18**, DOI: 10.1007/s00382-013-1768-y.

Christensen JH, Hewitson B, Busuioc A, Chen A, Gao X, Held I, Jones R, Kolli RK, Kwon W-T, Laprise R, Magaña Rueda V, Mearns L, Menéndez CG, Räisänen J, Rinke A, Sarr A, Whetton P, Tignor M. 2007. Regional climate projections. In *Climate Change 2007: The Physical Science Basis. Contribution of Working Group I to the 4th Assessment Report of the Intergovernmental Panel on Climate Change*, Solomon S, Qin D, Manning M, Chen Z, Marquis M, Averyt KB, Miller HL (eds). Cambridge University Press: Cambridge, UK.

Collini EA, Berbery EH, Barros VR, Pyle ME. 2008. How does soil moisture influence the early stages of the south American monsoon? *J. Clim.* **21**: 195–213, DOI: 10.1175/2007jcli1846.1.

Dirmeyer PA, Schlosser CA, Brubaker KL. 2009. Precipitation, recycling, and land memory: an integrated analysis. *J. Hydrometeorol.* **10**: 278–288, DOI: 10.1175/2008jhm1016.1.

Eltahir EAB. 1998. A soil moisture-rainfall feedback mechanism 1. Theory and observations. *Water Resour. Res.* **34**: 765–776.

Fernandez JPR, Franchito SH, Rao VB. 2006. Simulation of the summer circulation over South America by two regional climate models. Part I: mean climatology. *Theor. Appl. Climatol.* **86**(1–4): 247–260.

Jaeger EB, Seneviratne SI. 2011. Impact of soil moisture–atmosphere coupling on European climate extremes and trends in a regional climate model. *Clim. Dyn.* **36**(9–10): 1919–1939, DOI: 10.1007/s00382-010-0780-8.

Kain JS, Fritsch JM. 1993. Convective parameterizations for mesoscale models: The Kain-Fritsch scheme. In *The Representation of Cumulus Convection in Numerical Models*, Vol. 24, Meteorological Monograph, American Meteorological Society: Washington DC; 165–170.

Kjellström E, Bärring L, Gollvik S, Hansson U, Jones CG, Samuelsson P, Rummukainen M, Ullerstig A, Willén U, Wyser K. 2005. A 140-year simulation of European climate with the new version of the Rossby Centre regional atmospheric climate model (RCA3). Reports Meteorology and Climatology, Report No. 108, SMHI. Norrköping, Sweden.

Koster RD, Suarez MJ. 2001. Soil moisture memory in climate models. *J. Hydrometeorol.* **2**: 558–570, DOI: 10.1175/1525-7541(2001)002<0558:smmicm>2.0.co;2.

Koster RD, Guo Z, Dirmeyer PA, Bonan G, Chan E, Cox P, Davies H, Gordon CT, Kanae S, Kowalczyk E, Lawrence D, Liu P, Lu CH, Malyshev S, McAvaney B, Mitchell K, Mocko D, Oki T, Oleson KW, Pitman A, Sud YC, Taylor CM, Verseghy D, Vasic R, Xue Y, Yamada T. 2006. GLACE: The global land–atmosphere coupling experiment. Part I: overview. *J. Hydrometeorol.* **7**: 590–610, DOI: 10.1175/jhm510.1.

Ma HY, Mechoso CR, Xue Y, Xiao H, Wu CM, Li JL, de Sales F. 2011. Impact of land surface processes on the South American warm season climate. *Clim. Dyn.* **37**: 187–203, DOI: 10.1007/s00382-010-0813-3.

Makarieva AM, Gorshkov VG. 2007. Biotic pump of atmospheric moisture as driver of the hydrological cycle on land. *Hydrol. Earth Syst. Sci.* **11**: 1013–1033, DOI: 10.5194/hess-11-1013-2007.

Makarieva AM, Gorshkov VG, Sheil D, Nobre AD, Li BL. 2013. Where do winds come from? A new theory on how water vapor condensation influences atmospheric pressure and dynamics. *Atmos. Chem. Phys.* **13**: 1039–1056, DOI: 10.5194/acp-13-1039-2013.

Masson V, Champeaux JL, Chauvin F, Meriguet C, Lacaze R. 2003. A global database of land surface parameters at 1-km resolution in meteorological and climate models. *J. Clim.* **16**: 1261–1282, DOI: 10.1175/1520-0442-16.9.1261.

McGlone D, Vuille M. 2012. The associations between El Niño-Southern Oscillation and tropical South American climate in a regional climate model. *J. Geophys. Res. D: Atmos.* **117**(6), DOI: 10.1029/2011JD017066.

Menéndez CG, de Castro M, Boulanger JP, D'Onofrio A, Sanchez E, Sörensson AA, Blazquez J, Elizalde A, Jacob D, Le Treut H, Li ZX, Núñez MN, Pessacg N, Pfeiffer S, Rojas M, Rolla A, Samuelsson P,

Solman SA, Teichmann C. 2010a. Downscaling extreme month-long anomalies in southern South America. *Clim. Change* **98**: 379–403, DOI: 10.1007/s10584-009-9739-3.

Menéndez CG, De Castro M, Sörensson A, Boulanger JP. 2010b. CLARIS project: Towards climate downscaling in South America. *Meteorol. Z.* **19**: 357–362, DOI: 10.1127/0941-2948/2010/0459.

Negrón Juárez RI, LiW FK, de Oliveira CA. 2009. Comparison of precipitation data sets over tropical South America and African continents. *J. Hydrometeorol.* **10**(1): 289–299, DOI: 10.1175/2008JHM1023.1.

New M, Hulme M, Jones P. 1999. Representing twentieth-century space-time climate variability. Part I: development of a 1961–90 mean monthly terrestrial climatology. *J. Clim.* **12**: 829–856.

New M, Hulme M, Jones P. 2000. Representing twentieth-century space-time climate variability. Part II: Development of 1901–1996 monthly grids of terrestrial surface climate. *J. Clim.* **13**: 2217–2238.

Nogués-Paegle J, Mechoso CR, Fu R, Berbery EH, Chao WC, Chen TC, Cook K, Diaz AF, Enfield D, Ferreira R, Grimm AM, Kousky V, Liebmann B, Marengo J, Mo K, Neelin JD, Paegle J, Robertson AW, Seth A, Vera CS, Zhou J. 2002. Progress in Pan American CLIVAR research: understanding the South American monsoon. *Meteorologica* **27**: 3–32.

Pielke RA Sr. 2001. Influence of the spatial distribution of vegetation and soils on the prediction of cumulus convective rainfall. *Rev. Geophys.* **39**: 151–177, DOI: 10.1029/1999rg000072.

Rasch PJ, Kristjansson JE. 1998. A comparison of the CCM3 model climate using diagnosed and predicted condensate parameterisations. *J. Clim.* **11**: 1587–1614.

Samuelsson P, Gollvik S, Ullerstig A. 2006. The land-surface scheme of the Rossby Centre regional atmospheric climate model (RCA3). Report in Meteorology 122, SMHI. Norrköping, Sweden.

Samuelsson P, Jones CG, Willén U, Ullerstig A, Gollvik S, Hansson U, Jansson C, Kjellström E, Nikulin G, Wyser K. 2011. The Rossby Centre Regional Climate model RCA3: model description and performance. *Tellus Ser. A: Dyn. Meteorol. Oceanogr.* **63**: 4–23, DOI: 10.1111/j.1600-0870.2010.00478.x.

Sass BH, Rontu L, Savijärvi H, Räisänen P. 1994. HIRLAM-2 Radiation scheme: Documentation and tests. Hirlam Technical Report No. 16, SMHI. Norrköping, Sweden, 43.

Saulo C, Ferreira L, Nogués-Paegle J, Seluchi M, Ruiz J. 2010. Land-atmosphere interactions during a northwestern Argentina low event. *Mon. Weather Rev.* **138**: 2481–2498, DOI: 10.1175/2010mwr3227.1.

Savijärvi H. 1990. A fast radiation scheme for mesoscale model and short-range forecast models. *J. Appl. Meteorol.* **29**: 437–447.

Seluchi ME, Marengo JA. 2000. Tropical–midlatitude exchange of air masses during summer and winter in South America: climatic aspects and examples of intense events. *Int. J. Climatol.* **20**: 1167–1190, DOI: 10.1002/1097-0088(200008)20:10<1167::aid-joc526>3.0.co;2-t.

Seneviratne SI, Corti T, Davin EL, Hirschi M, Jaeger EB, Lehner I, Orlowsky B, Teuling J. 2010. Investigating soil moisture-climate interactions in a changing climate: a review. *Earth Sci. Rev.* **99**(3–4): 125–161, DOI: 10.1016/j.earscirev.2010.02.004.

Siqueira JR, Machado LAT. 2004. Influence of the frontal systems on the day-to-day convection variability over South America. *J. Clim.* **17**: 1754–1766.

Solman SA, Sanchez E, Samuelsson P, da Rocha RP, Li L, Marengo J, Pessacg NL, Remedio ARC, Chou SC, Berbery H, Le Treut H, de Castro M, Jacob D. 2013. Evaluation of an ensemble of regional climate model simulations over South America driven by the ERA-Interim reanalysis: model performance and uncertainties. *Clim. Dyn.* **1–19**, DOI: 10.1007/s00382-013-1667-2.

Sörensson AA. 2010. *Analysis of Land Surface-Atmospheric Feedbacks in South America using a New Regional Climate Model*, PhD thesis, Universidad de Buenos Aires: Buenos Aires, Argentina.

Sörensson AA, Menéndez CG. 2011. Summer soil-precipitation coupling in South America. *Tellus Ser. A: Dyn. Meteorol. Oceanogr.* **63**: 56–68, DOI: 10.1111/j.1600-0870.2010.00468.x.

Sörensson AA, Menéndez CG, Samuelsson P, Willén U, Hansson U. 2010. Soil-precipitation feedbacks during the South American Monsoon as simulated by a regional climate model. *Clim. Change* **98**: 429–447, DOI: 10.1007/s10584-009-9740-x.

Spracklen DV, Arnold SR, Taylor CM. 2012. Observations of increased tropical rainfall preceded by air passage over forests. *Nature* **489**: 282–285, DOI: 10.1038/nature11390.

Taylor CM, Parker DJ, Harris PP. 2007. An observational case study of mesoscale atmospheric circulations induced by soil moisture. *Geophys. Res. Lett.* **34**, DOI: 10.1029/2007gl030572.

Uppala SM, Kållberg PW, Simmons AJ, Andrae U, da Costa BV, Fiorino M, Gibson JK, Haseler J, Hernandez A, Kelly GA, Li X, Onogi K, Saarinen S, Sokka N, Allan RP, Andersson E, Arpe K, Balmaseda MA, Beljaars ACM, van de Berg L, Bidlot J, Bormann N, Caires S, Chevallier F, Dethof A, Dragosavac M, Fisher M, Fuentes M, Hagemann S, Hólm E, Hoskins BJ, Isaksen L, Janssen PAEM, Jenne R, McNally AP, Mahfouf JF, Morcrette JJ, Rayner NA, Saunders RW, Simon P, Sterl A, Trenberth KE, Untch A, Vasiljevic D, Viterbo P, Woollen J. 2005. The ERA-40 reanalysis. *Q. J. Roy. Meteorol. Soc.* **131**: 2961–3012, DOI: 10.1256/qj.04.176.

Urrutia R, Vuille M. 2009. Climate change projections for the tropical Andes using a regional climate model: temperature and precipitation simulations for the end of the 21st century. *J. Geophys. Res. D: Atmos.* **14**(2), DOI: 10.1029/2008JD011021.

Velasco I, Fritsch JM. 1987. Mesoscale convective complexes in the Americas. *J. Geophys. Res.* **92**: 9591–9613.

Wang G, Kim Y, Wang D. 2007. Quantifying the strength of soil moisture-precipitation coupling and its sensitivity to changes in surface water budget. *J. Hydrometeorol.* **8**: 551–570, DOI: 10.1175/jhm573.1.

Wei J, Dirmeyer PA. 2010. Toward understanding the large-scale land–atmosphere coupling in the models: roles of different processes. *Geophys. Res. Lett.* **37**, DOI: 10.1029/2010gl044769.

Wilks DS. 2006. *Statistical Methods in the Atmospheric Sciences*. International Geophysics Series, 2nd edn. Academic Press (Elsevier): Massachusetts, MA; California, CA and London.

